ROYAL SOCIETY OF CHEMISTRY

COMMUNICATION

Check for updates

Solution-processed single-emissive-layer WOLEDs with high efficiency and ultra-high color rendering index beyond 90†

Dongling Zhou,‡[a] Gang Cheng, ‡*[abc] Weiqiang Liu,[ad] Siping Wu[a] and Chi-Ming Che *[abc]

White organic light-emitting diodes (WOLEDs) have appealing applications in display technology. Developing WOLEDs based on cost-effective manufacturing processes is critical to the commercial pursuits of this technology. Solution-processed WOLEDs (SP-WOLEDs) constructed with a single emissive layer (EML) are a worthy candidate for development. To achieve SP-WOLEDs with high efficiency and high color quality, it is necessary to maximize the exciton utilization efficiency and to regulate the energy transfer process. Herein, three-color SP-WOLEDs were devised, with an EML containing blue and orange luminescent Au(III) complexes and the deep-red emitter tetraphenyldibenzoperiflanthene (DBP). The optimized WOLED exhibited high maximum external quantum efficiency of 12.72%, attributable to the high exciton utilization efficiency realized by doping a blue thermally activated delayed fluorescent Au(III) emitter and restraining exciton loss by DBP. High-quality warm-white emission was attained, with Commission International de l'Éclairage coordinates of (0.40, 0.40), correlated color temperature of 3695 K, and color rendering index (CRI) of 93, fulfilling the indoor lighting requirements. This result is among the best values for the single-EML SP-WOLEDs with CRI > 90 reported in the literature.

1. Introduction

Organic light-emitting diodes (OLEDs) have great potential to be used in solid-state lighting and are presently used in full-color displays as a result of the rapid improvements in color quality, device efficiency, and operational stability of OLED devices over the past decade. White OLEDs (WOLEDs) emit a soft, diffused, and glare-free light that is more eye-protective than LEDs, rendering them a better human-centric light source.[1] In comparison to other light sources such as LEDs and fluorescent lamps, the prevalent fabrication technique for high-efficiency WOLEDs is thermal deposition under ultra-high vacuum, which suffers from high fabrication costs due to the harsh fabrication conditions and complicated procedures required for sophisticated device architecture. In this regard, solution-processed techniques, such as spin-coating, inkjet printing, and roll-to-roll printing, could effectively lower the cost of WOLED fabrication while allowing greater ease of processing.[2] The device structure of solution-processed WOLEDs (SP-WOLEDs) is typically more simplified than that of vacuum-deposited counterparts. A single emissive layer (EML) composed of all host(s) and emitting dopants is usually employed in SP-WOLEDs, being different from multiple EMLs (in a single cell or tandem structure) with different emitters located in separated EMLs that are often utilized in vacuum-deposited WOLEDs.[1g] The simplified device fabrication could reduce manufacturing costs and enable mass production of large-area displays.

The key factors in evaluating the performance of WOLEDs include device efficiency and white color quality. The color quality of a white-light source can be quantified using the color rendering index (CRI), which is a measure of a light source's ability to manifest the true color of an object relative to a natural light source.[1g] Both general CRI and specific CRI R9 values are decisive parameters for evaluating the color rendering performance of WOLEDs. For instance, the ENERGY STAR program requires that the general CRI should be larger than 80 and the CRI R9 should be positive for Integral LED Lamps.[3] One simple strategy for developing white emission is to combine two colors of blue with either orange or red light.[4] The CRI values of these two-color SP-WOLEDs are generally less than 80 due to insufficient coverage of the visible region. The integration of

a State Key Laboratory of Synthetic Chemistry, Department of Chemistry, The University of Hong Kong, Pokfulam Road, Hong Kong SAR, China. E-mail: ggcheng@hku.hk, cmche@hku.hk

b Chemistry and Chemical Engineering Guangdong Laboratory, Shantou, 515041, Guangdong, China

c Hong Kong Quantum AI Lab Limited, 17 Science Park West Avenue, Pak Shek Kok, Hong Kong SAR

d State Key Laboratory of Rare Earth Resource Utilization, Changchun Institute of Applied Chemistry, Chinese Academy of Science, Changchun, 130022, China

‡ Dongling Zhou and Gang Cheng contributed equally to this work.

three or more emission colors is effective to construct SP-WOLEDs with CRI $\geq$ 90 by covering the entire visible range.[5] For example, Bradley *et al.* developed a panel of blue-, green-, and red-emitting polymers featuring electroluminescence (EL) located at 455 nm, 535 nm, and 620 nm, respectively.[5a] Benefiting from the broad EL spectra of green- and red-emitting polymers, the three-color WOLED achieved Commission International de l'Éclairage (CIE) coordinates of (0.36, 0.37) and CRI of 91. However, due to the internal quantum efficiency of these fluorescent polymers being limited to no more than 25%, the as-fabricated WOLED showed a relatively low maximum current efficiency (CE_{max}) of 9.8 cd A^{-1}. To attain a continuous EL spectrum across the whole visible range, Wong *et al.* applied three iridium(III) phosphors and a blue-emitting polymer into a single EML to realize SP-WOLEDs, where the polymer acted as both a host and a blue dopant.[5b] The optimized hybrid device exhibited maximum external quantum efficiency (EQE_{max}) of 12.6% and pure white emission with CIE coordinates of (0.36, 0.33) and CRI of 90. Huang *et al.* demonstrated an SP-WOLED with four iridium(III) complexes co-doped into an EML.[5c] The EL spectrum of the WOLED encompassed the whole visible region, generating warm white emission with CIE coordinates of (0.45, 0.44) and CRI of 91. Nonetheless, a relatively low power efficiency (PE_{max}) of 9.6 lm W^{-1} was recorded. Despite high-quality white electroluminescence being achieved, the device efficiencies of single-EML SP-WOLEDs reported so far are still significantly lower than those of vacuum-deposited WOLEDs.[1g,4h,5]

The utilization of a blue thermally activated delayed fluorescent (TADF) material as both a sensitizer and an emissive dopant is becoming a promising solution for high-performance WOLEDs, since these WOLEDs would benefit from TADF emitters having fast reverse intersystem crossing that enable the full harvesting of singlet and triplet excitons, realizing theoretical unitary internal quantum efficiencies, and from their broadband emission with a large full-width-at-half-maximum (FWHM) of $\approx$100 nm, allowing for high color rendering properties.[4c,d,6] In our previous study, a Au(III)-TADF sky-blue emitter, **Au-1**, was reported to demonstrate decent EL performance.[7] The SP-OLED based on 6 wt% **Au-1** exhibited EQE_{max} of 15.3% and CIE coordinates of (0.16, 0.25). With increasing the concentration of **Au-1** to 12 wt%, the EQE_{max} was as high as 12.4%, revealing that concentration-induced emission quenching of **Au-1** at high doping concentrations was minor. This is important for the use of **Au-1** as a blue sensitizer in WOLEDs, where the blue sensitizer is always highly doped in order to achieve white emission.

To generate high-CRI white emission, besides the blue emission color, it is indispensable to have emission of two other primary colors. In this work, **Au-1** was used as an energy donor, and an orange-emitting Au(III) complex **Au-7** (or **Au-8**)[8] and a deep-red emitter tetraphenyldibenzoperiflanthene (DBP) were chosen as energy acceptors (Scheme 1). These emitters were co-doped into a single EML to construct three-color SP-WOLEDs. Although the combined use of these emitting materials can guarantee a broad EL spectrum over the whole visible region for high color rendering performance, DBP is a conventional fluorescent emitter with only singlet excitons (= 25% of total excitons) responsible for
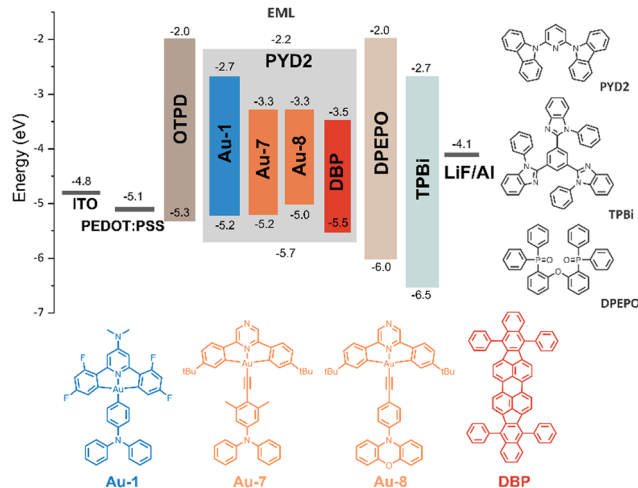
Scheme 1 Schematic device structure of single-EML SP-OLEDs with proposed energy level diagrams and chemical structures of emitting dopants and selected supportive materials used in the device fabrication.

the EL emission process, and triplet exciton generation in DBP would sacrifice device efficiency. In such a single-EML structure, Dexter-type triplet to triplet energy transfer from the sensitizer to DBP is inevitable, and direct charge trapping on DBP might also cause triplet exciton loss.

These issues may be circumvented by doping DBP at extremely low concentrations ($<$1 wt%). As Dexter energy transfer relies on a short-range electron exchange mechanism that requires significant orbital overlap between adjacent molecules, reducing the concentration of DBP could effectively increase the intermolecular distance between DBP and the sensitizer, thereby suppressing the undesired Dexter energy transfer process. Meanwhile, lightly doped DBP could help to restrain charge recombination on DBP. In this regard, efficient Förster resonance energy transfer (FRET) from the Au(III) sensitizer to DBP is required so that white-light emission could be accomplished by blending with lightly doped DBP. The energy transfer from the Au(III) sensitizer to DBP was studied in this work, and three-color WOLEDs have been developed with a low concentration of DBP optimized to 0.25 wt%. A high EQE_{max} of 12.72% and warm-white emission with CIE coordinates of (0.40, 0.40), correlated color temperature (CCT) of 3695 K, and ultra-high CRI of 93 at 1000 cd m^{-2} were achieved for the optimized WOLED with 10 wt% **Au-1**, 1 wt% **Au-7**, and 0.25 wt% DBP. Notably, the EQE_{max} of the three-color WOLED (12.72%) is comparable to that of the monochromatic device based on 10 wt% **Au-1** (12.91%),[7] indicative of a similar exciton utilization efficiency being achieved in the current WOLED and the successful suppression of DBP-related triplet exciton quenching.

2. Results and discussion

2.1 Photophysical properties of Au-1, Au-7, and Au-8

Complexes **Au-1**, **Au-7**, and **Au-8** were synthesized according to established protocols[7,8] and their characterization data are given in the ESI.† **Au-1** is an efficient blue TADF emitter, featuring emission λ_{max} at 484–495 nm with high emission

This journal is © The Royal Society of Chemistry 2023

J. Mater. Chem. C, 2023, **11**, 3936–3943 | **3937**

quantum yields (Φ) of $\approx 80\%$ and sub-microsecond radiative lifetimes (τ) in toluene solution and PMMA thin film. Complex **Au-7** and **Au-8** show TADF emission in the orange-red spectral region with Φ of 2–8% and τ of 0.2–0.3 μs in degassed toluene solution. The emission properties of **Au-7** and **Au-8** in thin films were also investigated. These two complexes showed stronger TADF emission in 10 wt% 2,6-di(9*H*-carbazol-9-yl)pyridine (PYD2) doped films than in toluene, showing broad emission bands with emission maxima at 564–592 nm and large FWHM of ≈ 100–120 nm, Φ of 28–63%, and τ of 1.03–1.25 μs (Fig. S1 and Table S1, ESI†).

2.2 Electroluminescent properties of Au-7 and Au-8

As shown in Scheme 1, the solution-processed OLEDs based on **Au-7** (or **Au-8**) were fabricated with a simple configuration of ITO/PEDOT:PSS/OTPD (4 nm)/PYD2: dopant(s) (60 nm)/DPEPO (10 nm)/TPBi (40 nm)/LiF (1.2 nm)/Al (100 nm), where PEDOT: PSS, OTPD, DPEPO, and TPBi refer to poly(3,4-ethylenedioxy-thiophene):poly(styrene sulfonate), *N*,*N'*-bis(4-(6-((3-ethyloxetan-3-yl)methoxy))-hexylphenyl)-*N*,*N'*-diphenyl-4,4'-diamine, bis(2-(diphenylphosphino)phenyl) ether oxide, and 1,3,5-tris(1-phenyl-1*H*-benzo[*d*]imidazol-2-yl)benzene, respectively. In these devices, PYD2 was utilized as the host for the emitting dopant(s) by virtue of its wide energy gap and high triplet energy level, while DPEPO and TPBi functioned as the hole/exciton blocking material and electron trans-porting material, respectively. An ultra-thin layer of cross-linkable OTPD was applied to facilitate hole injection into the EML due to its appropriate HOMO energy level of −5.3 eV lying between the hole injection layer (PEDOT:PSS, −5.1 eV) and EML (PYD2, −5.7 eV), and to prevent exciton quenching from the interface of PEDOT:PSS/EML.[9]

At 4 wt% of **Au-7**, the device showed a broad emission band peaking at 600 nm with a large FWHM of 110 nm, rendering orange emission with CIE coordinates of (0.45, 0.53) (Fig. 1a). Increasing the doping concentration of **Au-7** to 10 wt% resulted in a red-shifted emission maximum by 11 nm, with CIE coordinates of (0.50, 0.49). A higher EQE$_{max}$ of 14.22% was achieved for the 4 wt% **Au-7**-based device (Fig. 1b). A similar broad EL spectrum with CIE coordinates of (0.44, 0.54) was demonstrated in the device fabricated with 4 wt% **Au-8**. The same device exhibited an inferior EQE$_{max}$ of 10.87% relative to the 4 wt% **Au-7**-based device, likely due to the lower emission quantum yield of **Au-8** doped in PYD2 thin films (Table S1, ESI†). As portrayed in Fig. S1 (ESI†), the emission profiles of **Au-7** and

Au-8 doped in PYD2 thin films are comparable to their respective EL spectra. The broad emission bands and good device efficiency featured by these Au(III) emitters in SP-OLEDs render them suitable for use in SP-WOLED fabrication.

2.3 Complementary two-color WOLEDs based on Au(III) complexes

Combination of emitters with complementary emission colors, typically blue and orange ones, has been a strategy used in the fabrication of WOLEDs.[4c,h,i] In this study, **Au-1**, a reported Au(III)-TADF blue emitter, was incorporated into the single EML of **Au-7**- or **Au-8**-based devices to construct complementary two-color WOLEDs. As the emission spectrum of **Au-1** has good spectral overlap with the absorption spectrum of **Au-7** (or **Au-8**) (Fig. S3, ESI†), ET from **Au-1** to **Au-7** (or **Au-8**) would take place. To quantify the effectiveness of the ET process, the Förster distances (R_{FRET}) of the investigated donor–acceptor systems were calculated using the equation given in the ESI.† The large R_{FRET} of 3.02 nm for **Au-1**/**Au-7** and 2.28 nm for **Au-1**/**Au-8** reveals that the FRET from **Au-1** to **Au-7** (or **Au-8**) is efficient at low acceptor concentrations. To develop WOLEDs, the doping concentration of **Au-1** was fixed at 10 wt% relative to the PYD2 host, while those of **Au-7** and **Au-8** were optimized to 0.5 or 1 wt%. Fig. 2a depicts the EL spectra of the devices based on **Au-1** and **Au-7** (or **Au-8**) at varying doping concentrations. These devices showed white-light electroluminescence with broad EL spectra spanning from 410 to 780 nm, with the blue emission at 470 nm from **Au-1** and the orange emission at around 550 nm from **Au-7** (or **Au-8**). By tuning the doping concentration of **Au-7** (or **Au-8**) from 0.5 to 1 wt%, the orange emission became
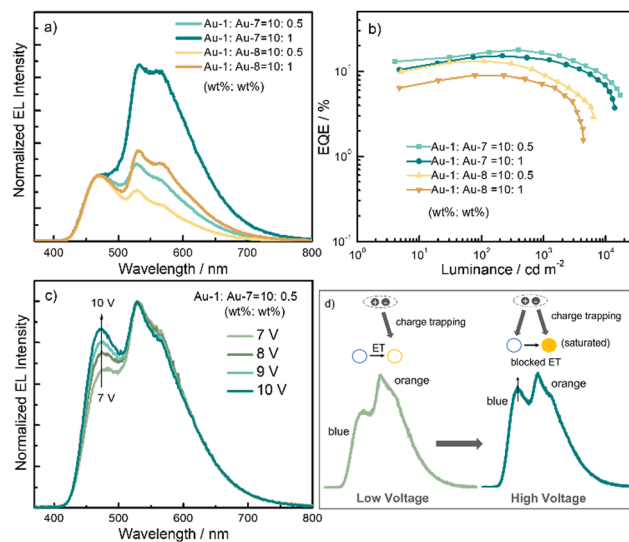
Fig. 2 (a) Normalized EL spectra and (b) EQE−luminance characteristics of complementary two-color WOLEDs based on **Au-1** and **Au-7** (or **Au-8**) at different doping concentrations; (c) normalized EL spectra of the **Au-1**:**Au-7**-based WOLED at different driving voltages; (d) schematic diagram of the proposed emission mechanisms of two-color WOLEDs at low and high voltages. The blue and orange hollow circles represent high-energy and low-energy emitters, respectively; the orange solid circle at high voltage stands for the low-energy emitter with saturated excited states.

Fig. 1 (a) EL spectra and (b) EQE−luminance characteristics of devices based on **Au-7** (or **Au-8**) at different doping concentrations.

3938 | *J. Mater. Chem. C*, 2023, **11**, 3936–3943

This journal is © The Royal Society of Chemistry 2023

stronger relative to the blue emission, with CIE coordinates shifting from (0.30, 0.40) to (0.37, 0.47) for the devices with **Au-7** and from (0.26, 0.35) to (0.32, 0.42) for the devices containing **Au-8**. At the same doping concentration, the **Au-1** : **Au-7**-based devices afforded higher orange emission intensity in the resulting white emission than the devices with **Au-8**, indicating more efficient ET from **Au-1** to **Au-7** than to **Au-8**. The CRI of the devices fabricated with 0.5 wt% **Au-7** (71), 0.5 wt% **Au-8** (72), and 1 wt% **Au-8** (71) was higher than that of the device with 1 wt% **Au-7** (63) (Table 1). The higher CRI is attributed to a more even distribution of the intensity of blue and orange emission.

The EQE–luminance and key performance characteristics of these complementary WOLEDs are shown in Fig. 2b and Table 1. Among them, a better performance was obtained for the device made from 10 wt% **Au-1** and 0.5 wt% **Au-7**, showing EQE_{max} of 17.84%, PE_{max} of 49.78 lm W^{-1}, and L_{max} of 17 300 cd m^{-2}. The PE_{max} was close to that of fluorescence lamps (40–70 lm W^{-1}). Moreover, at a high luminance of 1000 cd m^{-2}, the EQE still remained at 16.45%, corresponding to a small efficiency roll-off of 7.79%. For comparison, a device containing 0.5 wt% **Au-7** only was also fabricated. In this single-dopant device, the emission arising from the PYD2 host was observed with an EL peak at 380 nm (Fig. S4a, ESI†), revealing that the ET from PYD2 to **Au-7** was inefficient; a low EQE_{max} of 8.32% was therefore recorded (Fig. S4b, ESI†). When 10 wt% **Au-1** was introduced, the PYD2 emission vanished, indicative of a cascade ET process from PYD2 to **Au-7** through **Au-1**. Such ET was also evidenced by the PL decay curves of co-doped films monitored at the emission peak (482 nm) of **Au-1**. As shown in Fig. S5b (ESI†), when compared with the emission decay time of 10 wt% **Au-1**-doped PYD2 thin film, a sharp decrease in emission lifetime was observed for the blended films of **Au-1** (10 wt%) : **Au-7** (0.5–1 wt%), validating the ET process from **Au-1** to **Au-7**.

The EL spectrum of the device based on 10 wt% **Au-1** and 0.5 wt% **Au-7** was found to vary significantly with the applied voltage. As shown in Fig. 2c, with increased driving voltage, the blue emission showed an increase in intensity relative to the orange emission, leading to a color shift. Such a voltage-dependent spectral change in single-EML devices could be rationalized by the competition between charge trapping and energy transfer through the EML (Fig. 2d).[10] Since **Au-1** and **Au-7** have lower LUMO and higher HOMO energy levels than the PYD2 host (Scheme 1), the EL process allows direct trapping of holes and electrons and subsequent exciton formation on these Au(III) emitters. In such a charge-trapping-controlled device, charges are prone to being trapped by **Au-7** at low voltage due to the lower LUMO level of **Au-7** (−3.3 eV) compared with **Au-1** (−2.7 eV). Both direct charge trapping and ET should be the emission mechanisms contributing to the resulting EL spectra. As depicted in Fig. S6 (ESI†), the current density decreased with increasing doping concentration of **Au-7** at the same driving voltage, which is usually an indicator of charge trapping on low-energy emitters.[11] With further increase of the driving voltage, the low-energy traps of **Au-7** may become saturated with injected carriers, resulting in the hindered ET from **Au-1** to **Au-7**; meanwhile, the possibility of charge trapping on **Au-1** is increased. Both effects might lead to a stronger blue emission of **Au-1** with increased driving voltage.

2.4 Three-color WOLEDs with high color quality

As the CRI of two-color WOLEDs is still below the requirement for indoor-lighting applications (CRI ≥ 80)[1c] and their CRI R_9 values are far from satisfaction, compensation for red color in the visible spectral region is necessary for achieving high-color-quality white emission. In this work, a deep-red emitter DBP was embedded in the EML of **Au-1** : **Au-7**-based devices in the fabrication of three-color WOLEDs having expanded coverage in the visible spectral region. Although DBP emission could

Table 1 Key parameters of SP-OLEDs studied in this work

Concentration of **Au-1** : **Au-Y**[a] : DBP (wt%)	L_{max}[b] (cd m^{-2})	V_{on}[b] (V)	EQE[e] (%)		CE_{max}[d] (cd A^{-1}); PE_{max}[d] (lm W^{-1})	CIE (x, y)[e]	CRI[f]; CRI R_9[f]
			Max	At 1000 cd m^{-2}			
0 : 4 (**Au-7**) : 0	10 500	3.5	14.22	11.30	41.84; 30.49	0.45, 0.53	50; −69
0 : 10 (**Au-7**) : 0	15 500	3.0	13.26	10.18	33.50; 26.30	0.50, 0.49	N/A
0 : 4 (**Au-8**) : 0	3720	4.0	10.87	5.25	34.48; 21.67	0.44, 0.54	44; −92
0 : 10 (**Au-8**) : 0	5750	3.8	8.48	5.07	23.61; 14.85	0.47, 0.51	49; −60
10 : 0.5 (**Au-7**) : 0	17 300	3.7	17.84	16.45	49.78; 30.63	0.30, 0.40	71; −49
10 : 1 (**Au-7**) : 0	14 000	3.7	15.21	13.83	45.83; 27.96	0.37, 0.47	63; −85
10 : 0.5 (**Au-8**) : 0	6330	3.7	13.15	8.89	36.17; 25.01	0.26, 0.35	72; −42
10 : 1 (**Au-8**) : 0	4330	3.7	9.00	7.12	26.90; 16.89	0.32, 0.42	71; −50
0 : 1 (**Au-7**) : 0.25	5500	3.6	8.76	7.80	22.58; 16.20	0.48, 0.49	65; −35
0 : 4 (**Au-7**) : 0.25	7920	4.0	9.05	8.15	22.27; 16.12	0.50, 0.49	63; −33
0 : 10 (**Au-7**) : 0.25	10 800	3.4	10.34	9.53	21.59; 15.67	0.54, 0.45	69; −37
0 : 10 (**Au-7**) : 1	4500	3.8	5.68	4.50	8.82; 5.54	0.59, 0.41	N/A
10 : 0 : 0.25	4120	3.6	11.51	6.10	19.73; 13.76	0.19, 0.23	N/A
10 : 0.5 (**Au-7**) : 0.25	8400	3.5	9.74	6.08	20.84; 16.09	0.34, 0.37	91; 59
10 : 1 (**Au-7**) : 0.25	9430	3.6	12.72	9.95	28.51; 22.28	0.40, 0.40	93; 66
10 : 2 (**Au-7**) : 0.25	20 800	3.5	12.15	11.33	28.44; 17.82	0.46, 0.46	82; 10
10 : 1 (**Au-8**) : 0.25	6400	5.0	8.54	6.30	18.97; 16.70	0.38, 0.40	94; 47

[a] **Au-Y** stands for **Au-7** or **Au-8**; these emitters were doped into the PYD2 host in the EML. [b] Maximum luminance; turn-on voltages at a luminance of 1 cd m^{-2}. [c] External quantum efficiency. [d] Maximum current efficiency and power efficiency. [e] Commission International de l'Éclairage coordinates at 1000 cd m^{-2}. [f] The general CRI is calculated as the average of R_1 to R_8, and the scale of CRI is 0–100; the specific index CRI R_9 demonstrates the extent of spectral coverage of a light source in the red region; general CRI and CRI R_9 values were recorded at 1000 cd m^{-2}.

This journal is © The Royal Society of Chemistry 2023

*J. Mater. Chem. C*, 2023, **11**, 3936–3943 | **3939**

make up for the deficiency in the red spectral region and broaden the coverage of the EL spectrum, the limitation of DBP in having only up to 25% internal quantum efficiency would reduce the EQEs of the resulting WOLEDs. To achieve high device efficiencies, DBP-involved triplet exciton quenching processes should be avoided, and the DBP emission should primarily come from the FRET process. Hence, efficient FRET from the Au(III) sensitizer to DBP is thus essential for high-efficiency WOLEDs. The ET from the Au(III) sensitizers to DBP was therefore investigated. Given that the spectral overlap between the emission spectrum of **Au-7** and absorption spectrum of DBP is larger than that between **Au-1** and DBP (Fig. S7, ESI†), the calculated R_{FRET} for **Au-7** and DBP (5.13 nm) is larger than that for **Au-1** and DBP (3.72 nm), suggesting ET from **Au-7** to DBP to be more efficient. Two comparable devices of blending 0.25 wt% DBP with either 10 wt% **Au-1** or 10 wt% **Au-7** in an EML were first examined. As shown in Fig. 3a, the **Au-1** : DBP device exhibited primarily blue EL corresponding to the emission from **Au-1** and its EQE$_{max}$ of 11.51% was slightly lower than that of the device with 10 wt% **Au-1** only (EQE$_{max}$ = 12.91%).[7] For the **Au-7** : DBP-based device, a broad EL spectrum was recorded, with an emission peak at 610 nm from DBP and a shoulder at $\approx$ 550 nm from **Au-7**. A high EQE$_{max}$ of 10.34% was achieved,

which exceeded the theoretical upper limit of EQE$_{max}$ ($\approx$ 5%) for conventional fluorescence-based OLEDs without the use of any light out-coupling enhancement technique.

A more detailed investigation of the ET from **Au-7** to DBP was then performed. Fig. 3b and c depict the EL spectra and EQE–luminance curves of the devices with different blend ratios of DBP and **Au-7**. When the concentration of **Au-7** was increased from 1 to 10 wt%, the EL intensity of **Au-7** gradually decreased relative to that of DBP whose concentration was fixed at 0.25 wt%; meanwhile, there was an increase in EQE$_{max}$ from 8.76 to 10.34%. For the device based on 10 wt% **Au-7** and 1 wt% DBP, the DBP emission with λ_{max} at 610 nm dominated the EL spectrum and the EQE$_{max}$ dropped to 5.68%. The largely sacrificed EQE may be due to exciton loss *via* mechanisms like direct charge trapping on DBP molecules and Dexter energy transfer involving highly doped DBP. These mechanisms would lead to DBP having more triplet excitons, hence resulting in more severe non-radiative depletion. The following findings are supportive of the described exciton loss mechanisms: (1) as shown in Fig. S8 (ESI†), the PL spectrum of the **Au-7** (10 wt%) : DBP (1 wt%) doped film was different from the respective EL spectrum; only DBP emission could be observed in the PL profile; and (2) the current density dropped at a given voltage with increasing DBP concentrations from 0.25 wt% to 1 wt% (Fig. S9a, ESI†). On the one hand, since energy transfer was the main mechanism responsible for DBP emission during the PL process, the difference in the PL and EL spectra is indicative of the contribution of charge trapping to the EL process; on the other hand, the reduced current density at high DBP concentrations reveals that the charges injected into the EML were more likely to be trapped by DBP.

Due to the efficient ET processes from **Au-1** to **Au-7** and from **Au-7** to DBP, a cascade energy transfer from **Au-1** to DBP through **Au-7** is proposed for the three-color WOLEDs. The suggested energy transfer process was confirmed by the shortened emission lifetime recorded at 482 nm, from 0.19 µs for the **Au-1** (10 wt%) : DBP (0.25 wt%) co-doped film to 0.14 µs after co-doping with 1 wt% **Au-7** (Fig. S10, ESI†). The DBP concentration in the WOLEDs was set at 0.25 wt% in order to control the exciton loss induced by unwanted charge trapping and Dexter energy transfer processes involving DBP. Manipulating the concentration of **Au-7** was used to tune the EL spectrum for white emission by influencing the ET rate of **Au-1**/**Au-7** and **Au-7**/DBP. As expected, for the devices with a single EML of **Au-1** (10 wt%) : **Au-7** (0.5–2 wt%) : DBP (0.25 wt%), increasing the concentration of **Au-7** from 0.5 to 2 wt% resulted in a decrease of the emission intensity of **Au-1** at 470 nm relative to that of DBP at 610 nm (Fig. 3d), accompanied by moving the CIE coordinates and CCT from a cool-white region of (0.34, 0.37) and 5231 K to a warm-white region of (0.46, 0.46) and 3058 K. Such a color shift is attributed to more efficient ET from **Au-1** to DBP through **Au-7** upon increasing the **Au-7** concentration, leading to a reduction of the blue-emission intensity in the resulting EL spectra.

Table 1 and Fig. 3e show the key EL performance of these three-color WOLEDs. Among these devices, the WOLED with 1 wt% **Au-7** demonstrated superior device efficiency and white
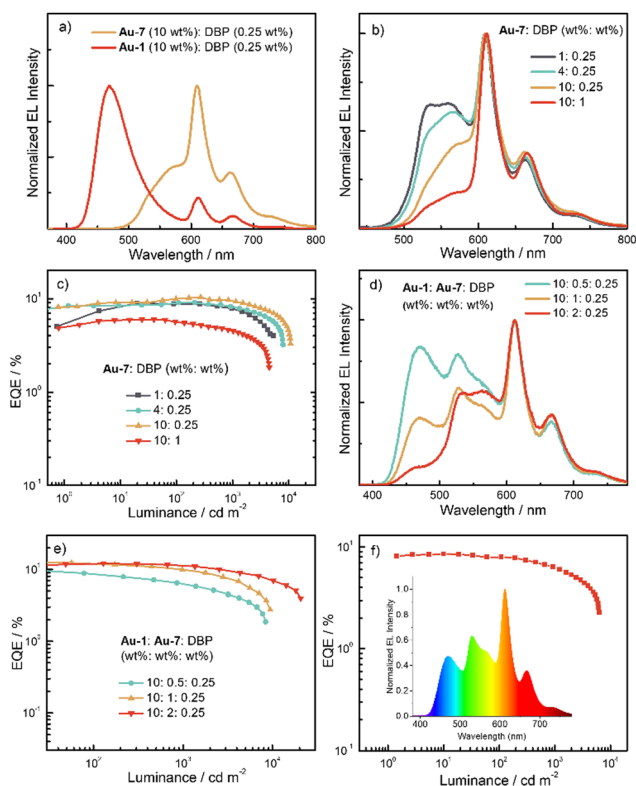
Fig. 3 (a) The EL spectra of devices with 0.25 wt% DBP and 10 wt% **Au-1** (or **Au-7**); (b) the EL spectra of devices with different blend ratios of DBP and **Au-7** and (c) their respective EQE–luminance characteristics; (d) the EL spectra of devices with different concentrations of **Au-1**, **Au-7**, and DBP and (e) their corresponding EQE–luminance characteristics; (f) EQEs as a function of luminance for the device based on 10 wt% **Au-1**, 1 wt% **Au-8**, and 0.25 wt% DBP (inset: the EL spectrum of the studied device).

Fig. 4 (a) Normalized EL spectra of the device based on **Au-1** (10 wt%), **Au-7** (1 wt%), and DBP (0.25 wt%) at different driving voltages (inset: the photo of the device taken at 6 V); (b) 2D AFM image (10 × 10 µm^2) with R_a and RMS values of the 10 wt% **Au-1** : 1 wt% **Au-7** : 0.25 wt% DBP blend film.

emission quality with EQE$_{max}$ of 12.72%, CIE coordinates of (0.40, 0.40), CRI of 93, and CRI R$_9$ of 66. Notably, this optimal WOLED showed a comparable EQE$_{max}$ as the monochromatic device with 10 wt% **Au-1** (EQE$_{max}$ = 12.91%),[7] revealing that a similar exciton utilization efficiency has been achieved and triplet exciton quenching by DBP might be largely suppressed in a single-EML device structure under the optimized dopant concentrations. Another WOLED with an EML of **Au-1** (10 wt%) : **Au-8** (1 wt%) : DBP (0.25 wt%) was fabricated, and its EL spectrum and EQE–luminance curve are plotted in Fig. 3f. The device exhibited high-quality white-light emission with CIE coordinates of (0.38, 0.40), CCT of 4163 K, and CRI of 94, but it showed a lower EQE$_{max}$ of 8.54% compared with the three-color WOLED with 1 wt% **Au-7**. The performance of the three-color WOLED with 1 wt% **Au-7**, to the best of our knowledge, is one of the best results among the reported single-EML SP-WOLEDs with CRI > 90 (Table S3, ESI†).[5] Even when compared with vacuum-deposited multiple-EML WOLEDs having CRI above 90, the EQE$_{max}$ achieved by this SP-WOLED is among the best values (Table S4, ESI†).[12]

Fig. 4a shows the variation of the EL spectra with increasing driving voltage for the device based on 10 wt% **Au-1**, 1 wt% **Au-7**, and 0.25 wt% DBP. When the driving voltage was increased from 6 to 10 V, the relative intensity of the emission at 470 nm slightly increased, with CIE coordinates shifting from (0.40, 0.40) at 1000 cd m^{-2} to (0.42, 0.42) at 9500 cd m^{-2} and CRI remaining above 90. These CIE coordinates lie within the warm-white-light region with CCT of 3400–3700 K (Fig. S13, ESI†). The considerable color stability might be attributable to the short emission lifetime and low doping concentration of DBP, which could mitigate the effect of charge trapping on DBP. The phase morphology and film-forming capability are also important parameters that affect the device performance of SP-OLEDs, particularly in host–guest systems. Fig. 4b shows 10 × 10 µm^2 top-view atomic force microscope (AFM) images of a co-doped film made with 10 wt% **Au-1**, 1 wt% **Au-7**, and 0.25 wt% DBP in the PYD2 host. There was no obvious phase separation or aggregation observed. The uniform profile with small and similar average roughness (R_a = 0.31 nm) and root mean square roughness (RMS = 0.39 nm) is indicative of satisfactory film-forming properties in the doping system. This may be attributed to the good compatibility and
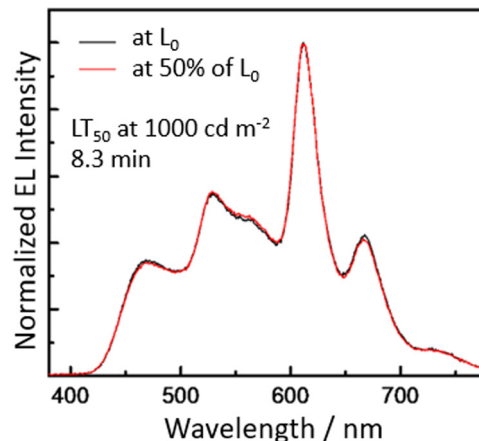

Fig. 5 Normalized EL spectra of the device based on **Au-1** (10 wt%), **Au-7** (1 wt%), and DBP (0.25 wt%) recorded before (black line) and after (red line) the device lifetime evaluation.

morphological stability between the host and emitting dopants at the respective concentrations used. The homogeneous morphology might contribute to the high device efficiency and color-stable white electroluminescence of the optimized WOLED.

The operational lifetimes of two WOLEDs based on 10 wt% **Au-1**, 1 wt% **Au-7** (or **Au-8**), and 0.25 wt% DBP were measured under our laboratory conditions using the device architecture shown in Scheme 1. As depicted in Fig. S16a and S17a (ESI†), at an initial luminance (L_0) of 1000 cd m^{-2}, the 1 wt% **Au-7**-based WOLED demonstrated an operational lifetime at 50% of the initial luminance (LT$_{50}$) of 8.3 min. For the 1 wt% **Au-8**-based WOLED, LT$_{50}$ was measured to be 10.2 min at an L_0 of 900 cd m^{-2}. The low operational stability may be due to the instability of PEDOT:PSS during continuous operation and the lack of optimization of the device structure for lifetime evaluation.[4d,13] Considering that WOLEDs with an operationally stable EL spectrum would appeal to lighting applications, the EL spectra of the aforementioned two WOLEDs were recorded before and after the device lifetime measurement. The normalized EL spectrum of the WOLED containing **Au-7** remained identical before and after the measurement (Fig. 5), whereas for the device with **Au-8**, the relative intensity of DBP emission became stronger after the lifetime evaluation (Fig. S17b, ESI†). The unchanged EL spectrum of the **Au-7**-based WOLED can be rationalized by the suppression of charge trapping on DBP and energy transfer as the primary emission mechanism. For the **Au-8**-based WOLED, the enhanced intensity of DBP emission may be due to the significant charge trapping on DBP on the basis of the less efficient ET from **Au-8** to DBP (R_{FRET} = 4.39 nm, Fig. S18, ESI†) compared with the ET from **Au-7** to DBP (R_{FRET} = 5.13 nm).

3. Conclusions

In summary, complementary two-color SP-WOLEDs with a single EML containing blue and orange emissive Au(III) emitters were devised. High-efficiency cool-white-light emission was attained with EQE$_{max}$ of 17.84%, PE$_{max}$ of 49.78 lm W^{-1}, CIE coordinates of

This journal is © The Royal Society of Chemistry 2023

J. Mater. Chem. C, 2023, **11**, 3936–3943 | **3941**

(0.30, 0.40), CCT of 6620 K, and CRI of 71. Three-color SP-WOLEDs have also been developed by incorporating a deep-red emitter DBP. A high exciton utilization efficiency was realized by impeding the DBP-related exciton quenching processes, and a high EQE_{max} of 12.72% was achieved for the optimized WOLED. High-quality warm-white emission was demonstrated for the same device, with CIE coordinates of (0.40, 0.40), CCT of 3695 K, CRI of 93, and CRI R_9 of 66, which meets the requirements for indoor lighting. In addition, this optimal WOLED exhibited considerable white emission stability with a small CIE deviation ΔCIE of (0.02, 0.02), CRI above 90, and CCT of 3400–3700 K over a wide range of luminance. The performance of three-color WOLED achieved in this work is among the best values for single-EML SP-WOLEDs having CRI > 90 reported in the literature. The present work unlocks the potential for the simultaneous realization of high device efficiency, high white emission quality, and high color stability in single-EML SP-WOLEDs.

Conflicts of interest

There are no conflicts to declare.

Acknowledgements

References

1 (a) J. Kido, M. Kimura and K. Nagai, *Science*, 1995, **267**, 1332–1334; (b) B. K. T. Kamtekar, A. P. Monkman and M. R. Bryce, *Adv. Mater.*, 2010, **22**, 572–582; (c) M. C. Gather, A. Köhnen and K. Meerholz, *Adv. Mater.*, 2011, **23**, 233–248; (d) S. Reineke, M. Thomschke, B. Lüssem and K. Leo, *Rev. Mod. Phys.*, 2013, **85**, 1245–1293; (e) J. Liang, L. Ying, F. Huang and Y. Cao, *J. Mater. Chem. C*, 2016, **4**, 10993–11006; (f) F. Zhao and D. Ma, *Mater. Chem. Front.*, 2017, **1**, 1933–1950; (g) Y. Yin, M. U. Ali, W. Xie, H. Yang and H. Meng, *Mater. Chem. Front.*, 2019, **3**, 970–1031.

2 (a) L. Duan, L. Hou, T.-W. Lee, J. Qiao, D. Zhang, G. Dong, L. Wang and Y. Qiu, *J. Mater. Chem.*, 2010, **20**, 6392–6407; (b) T. Tsujimura, J. Fukawa, K. Endoh, Y. Suzuki, K. Hirabayashi and T. Mori, *J. Soc. Inf. Disp.*, 2014, **22**, 412–418; (c) C. Li, *Inkjet Printing for AMOLED Technology & Market Report – 2019*, 2019.

3 ENERGY STAR® Program Requirements for Integral LED Lamps, 2011.

4 (a) Z. He, C. Wang, J. Zhao, X. Du, H. Yang, P. Zhong, C. Zheng, H. Lin, S. Tao and X. Zhang, *J. Mater. Chem. C*,
2019, **7**, 11806–11812; (b) J.-Y. Wu and S.-A. Chen, *ACS Appl. Mater. Interfaces*, 2018, **10**, 4851–4859; (c) M. Ma, J. Li, D. Liu, Y. Mei and R. Dong, *ACS Appl. Mater. Interfaces*, 2021, **13**, 44615–44627; (d) X. Chen, S. Wang, H. L. Lee, J. Y. Lee, X. Liao, L. Li, W. Zhu and Y. Wang, *Adv. Opt. Mater.*, 2021, **9**, 2101518; (e) C. Fan, Y. Lei, Z. Liu, R. Wang, Y. Lei, G. Li, Z. Xiong and X. Yang, *ACS Appl. Mater. Interfaces*, 2015, **7**, 20769–20778; (f) B. Zhang, G. Tan, C.-S. Lam, B. Yao, C.-L. Ho, L. Liu, Z. Xie, W.-Y. Wong, J. Ding and L. Wang, *Adv. Mater.*, 2012, **24**, 1873–1877; (g) G. Cheng, P.-K. Chow, S. C. F. Kui, C.-C. Kwok and C.-M. Che, *Adv. Mater.*, 2013, **25**, 6765–6770; (h) Y. Liu, X. Wei, Z. Li, J. Liu, R. Wang, X. Hu, P. Wang, T. Qi and Y. Wang, *Adv. Opt. Mater.*, 2018, **6**, 1800978; (i) S. Wang, D. Liu, X. Wu, L. Wang, J. Huang, J. Chen, Y. Wang and W. Zhu, *Appl. Phys. Lett.*, 2021, **119**, 153301; (j) J. Tagare, R. A. K. Yadav, S. S. Swayamprabha, D. K. Dubey, J.-H. Jou and S. Vaidyanathan, *J. Mater. Chem. C*, 2021, **9**, 4935–4947; (k) C. Li, Y. Xu, Y. Liu, Z. Ren, Y. Ma and S. Yan, *Nano Energy*, 2019, **65**, 104057.

5 (a) L. Yu, J. Liu, S. Hu, R. He, W. Yang, H. Wu, J. Peng, R. Xia and D. D. C. Bradley, *Adv. Funct. Mater.*, 2013, **23**, 4366–4376; (b) S. Hu, M. Zhu, Q. Zou, H. Wu, C. Yang, W.-Y. Wong, W. Yang, J. Peng and Y. Cao, *Appl. Phys. Lett.*, 2012, **100**, 063304; (c) N. Li, N. Zhang, Y. Quan, L. Li, S. Ye, Q. Fan and W. Huang, *Opt. Mater. Express*, 2018, **8**, 3208–3219; (d) J. Xu, L. Yu, Z. Sun, T. Li, H. Chen and W. Yang, *Org. Electron.*, 2020, **84**, 105785.

6 (a) Z. B. Wu, L. Yu, F. C. Zhao, X. F. Qiao, J. S. Chen, F. Ni, C. L. Yang, T. Ahamad, S. M. Alshehri and D. G. Ma, *Adv. Opt. Mater.*, 2017, **5**, 1700415; (b) J. Liang, C. L. Li, X. M. Zhuang, K. Q. Ye, Y. Liu and Y. Wang, *Adv. Funct. Mater.*, 2018, **28**, 1707002; (c) Q. Q. Liang, C. M. Han, C. B. Duan and H. Xu, *Adv. Opt. Mater.*, 2018, **6**, 1800020.

7 D. Zhou, G. Cheng, G. S. M. Tong and C.-M. Che, *Chem. – Eur. J.*, 2020, **26**, 15718–15726.

8 D. Zhou, W.-P. To, Y. Kwak, Y. Cho, G. Cheng, G. S. M. Tong and C.-M. Che, *Adv. Sci.*, 2019, **6**, 1802297.

9 K.-W. Tsai, M.-K. Hung, Y.-H. Mao and S.-A. Chen, *Adv. Funct. Mater.*, 2019, **29**, 1901025.

10 (a) M. C. Gather, R. Alle, H. Becker and K. Meerholz, *Adv. Mater.*, 2007, **19**, 4460–4465; (b) H. T. Nicolai, A. Hof and P. W. M. Blom, *Adv. Funct. Mater.*, 2012, **22**, 2040–2047.

11 M. Uchida, C. Adachi, T. Koyama and Y. Taniguchi, *J. Appl. Phys.*, 1999, **86**, 1680–1687.

12 (a) J. Kalinowski, M. Cocchi, D. Virgili, V. Fattori and J. A. G. Williams, *Adv. Mater.*, 2007, **19**, 4000–4005; (b) G. Zhou, Q. Wang, C.-L. Ho, W.-Y. Wong, D. Ma and L. Wang, *Chem. Commun.*, 2009, 3574–3576; (c) C.-H. Chang, K.-C. Tien, C.-C. Chen, M.-S. Lin, H.-C. Cheng, S.-H. Liu, C.-C. Wu, J.-Y. Hung, Y.-C. Chiu and Y. Chi, *Org. Electron.*, 2010, **11**, 412–418; (d) J.-H. Jou, S.-M. Shen, C.-R. Lin, Y.-S. Wang, Y.-C. Chou, S.-Z. Chen and Y.-C. Jou, *Org. Electron.*, 2011, **12**, 865–868; (e) J.-H. Jou, Y.-C. Chou, S.-M. Shen, M.-H. Wu, P.-S. Wu, C.-R. Lin, R.-Z. Wu, S.-H. Chen, M.-K. Wei and C.-W. Wang, *J. Mater. Chem.*,

3942 | *J. Mater. Chem. C*, 2023, **11**, 3936–3943

This journal is © The Royal Society of Chemistry 2023

2011, **21**, 18523–18526; (*f*) S. Chen, G. Tan, W.-Y. Wong and H.-S. Kwok, *Adv. Funct. Mater.*, 2011, **21**, 3785–3793; (*g*) Y. Li, W. Zhang, L. Zhang, X. Wen, Y. Yin, S. Liu, W. Xie, H. Zhao and S. Tao, *Org. Electron.*, 2013, **14**, 3201–3205; (*h*) T. Zhang, S.-J. He, D.-K. Wang, N. Jiang and Z.-H. Lu, *Sci. Rep.*, 2016, **6**, 20517; (*i*) B. Liu, H. Tao, L. Wang, D. Gao, W. Liu, J. Zou, M. Xu, H. Ning, J. Peng and Y. Cao, *Nano Energy*, 2016, **26**, 26–36; (*j*) Q. Sun, Y. Hu, Y. Dai and D. Ma, *J. Mater. Chem. C*, 2017, **5**, 8022–8026; (*k*) Y. Miao, K. Wang, B. Zhao, L. Gao, Y. Wang, H. Wang, B. Xu and F. Zhu, *J. Mater. Chem. C*,

2017, **5**, 12474–12482; (*l*) L. Gao, Z. Gao, K. Wang, Y. Miao, Y. Zhao, W. Jia, Y. Zhou, H. Wang and B. Xu, *J. Lumin.*, 2018, **201**, 224–230; (*m*) B. Wang, Z. Kou, Y. Tang, F. Yang, X. Fu and Q. Yuan, *Org. Electron.*, 2019, **70**, 149–154; (*n*) B. Wang, Z. Kou, Q. Yuan, X. Fu, Z. Fan and A. Zhou, *Org. Electron.*, 2020, **78**, 105617.

13 (*a*) G. Kreiza, D. Berenis, D. Banevičius, S. Juršėnas, T. Javorskis, E. Orentas and K. Kazlauskas, *Chem. Eng. J.*, 2021, **412**, 128574; (*b*) D. Zhou, S. Wu, G. Cheng and C.-M. Che, *J. Mater. Chem. C*, 2022, **10**, 4590.